Model of T-Cell Nuclear Deformation by the Cortical Actin Layer

Gur Fabrikant,[†△] Soumya Gupta,[‡△] G. V. Shivashankar,[‡*] and Michael M. Kozlov[†*]
[†]Department of Physiology and Pharmacology, Sackler Faculty of Medicine, Tel Aviv University, Ramat Aviv, Tel Aviv, Israel; and
[‡]Mechanobiology Institute and Department of Biological Sciences, National University of Singapore, Singapore

ABSTRACT Deformations of cell nuclei accompany a number of essential intracellular processes. Although evidence is being accumulated on the primary role actin structures play in controlling the shape of the nucleus, the mechanisms behind this phenomenon remain unknown. Here, we consider theoretically a specific paradigm of nuclear deformation, and a related actin rearrangement, in T cells stimulated by contact with a bead covered by surrogate antigens. We suggest that the nucleus is deformed by the elastic forces developed within a cylindrical layer of polymerized actin, which is generated as a result of the receptor-mediated T-cell activation. We substantiate this proposal with a theoretical analysis of mutual deformations in the actin layer and the nucleus, which recovers the experimentally observed nuclear shapes. Furthermore, we evaluate the forces developed by the actin polymerization that drives the nuclear deformation. The model predicts the mode of actin polymerization generated by the surrogate antigens covering a bead and the values of the elastic moduli of the nuclear shell. We provide a qualitative experimental support for the model assumptions by visualizing the stages of nuclear shape change and the corresponding evolution of the cortical actin.

INTRODUCTION

Emerging evidence indicates the importance of mechanical behavior of the nucleus (1,2). Such behavior includes the elastic deformation and restoration of nuclear shape in processes such as stem cell differentiation, development, homeostasis, and regulation of gene expression (3–7). Actin plays an important role in regulating nuclear shape in these different systems. Embryonic stem cells have round nuclei and lack defined actin stress fiber organization, but the induction of differentiation is accompanied by progressive formation of a perinuclear actin cap (8,9). Furthermore, the induction of pluripotency in differentiated cells is accompanied by the elimination of the actin cap (8). In developing *Drosophila* embryos, the nuclear shape is spherical during early blastoderm stages, but postcellularization it becomes elongated (3,4). In adherent cells, the perinuclear actin cap exerts a compressive load on the nucleus and gives it a defined shape. Disruption of these actin fibers results in a bulging of the nucleus and an increase in its height (10). In addition, depolymerization of actin or microtubules perturbs the nuclear shape as, under normal conditions, these two cytoskeletal components apply compressive and contractile forces, respectively, on the nucleus (11). Supporting this, an alteration of cytoskeletal organization in endothelial cells was observed after plating them on defined micropatterns that correlated with nuclear shape and volume (12,13). To stabilize nuclear morphology, the actin cytoskeleton is linked to the nuclear lamina and chromatin via the SUN and KASH domain proteins (14,15). Disruption of these links results in disturbed organization of the perinuclear actin and nuclear morphology, as well as impaired transmission of mechanical forces to the nucleus (14). Together, these observations highlight the importance of actin-mediated regulation of nuclear shape and its genomic functions. At the same time, the physical mechanism of this phenomenon remains unknown.

A convenient system for studying the physics of nuclear shape change, as mediated by the actin cytoskeleton, is represented by activated T cells. T cells are nonadherent and have little polymerized actin in them. Upon stimulation of their T-cell receptors by antigen-presenting cells (APCs), the T cell's actin undergoes massive polymerization (16,17). In cells plated on surrogate antigen-coated coverslips, this leads to the generation, at the cell periphery, of submembrane actin-rich rings. These are associated with the extension of lamellipodia and cell spreading (18).

Recently, we studied the changes in nuclear shape that resulted from T-cell activation by antibody-coated paramagnetic beads, whose 4.5 μm size imitated that of the antigen-presenting cells (19). Upon binding of the beads to a T-cell surface, both the cell and its nucleus underwent substantial elongation. We presented evidence to show that polymerized actin, rather than microtubules or actomyosin contractility, were responsible for this phenomenon (19). These studies clearly indicated the importance of the actin cytoskeleton in regulating nuclear shape and size. However, the specific mechanisms of this phenomenon remained unexplored.

Here, we propose a quantitative mechanical model using antigen-coated beads to account for nuclear shape changes driven by the actin cytoskeleton during T-cell activation. We suggest that nuclear deformation is induced in this system by a submembrane cortical actin layer that undergoes remodeling into a hollow cylindrical shape after T-cell

Submitted February 20, 2013, and accepted for publication July 11, 2013.

△Gur Fabrikant and Soumya Gupta contributed equally to this work.

*Correspondence: shiva.gvs@gmail.com or michk@post.tau.ac.il

Editor: Leah Edelstein-Keshet.

0006-3495/13/09/1316/8 $2.00

http://dx.doi.org/10.1016/j.bpj.2013.07.024

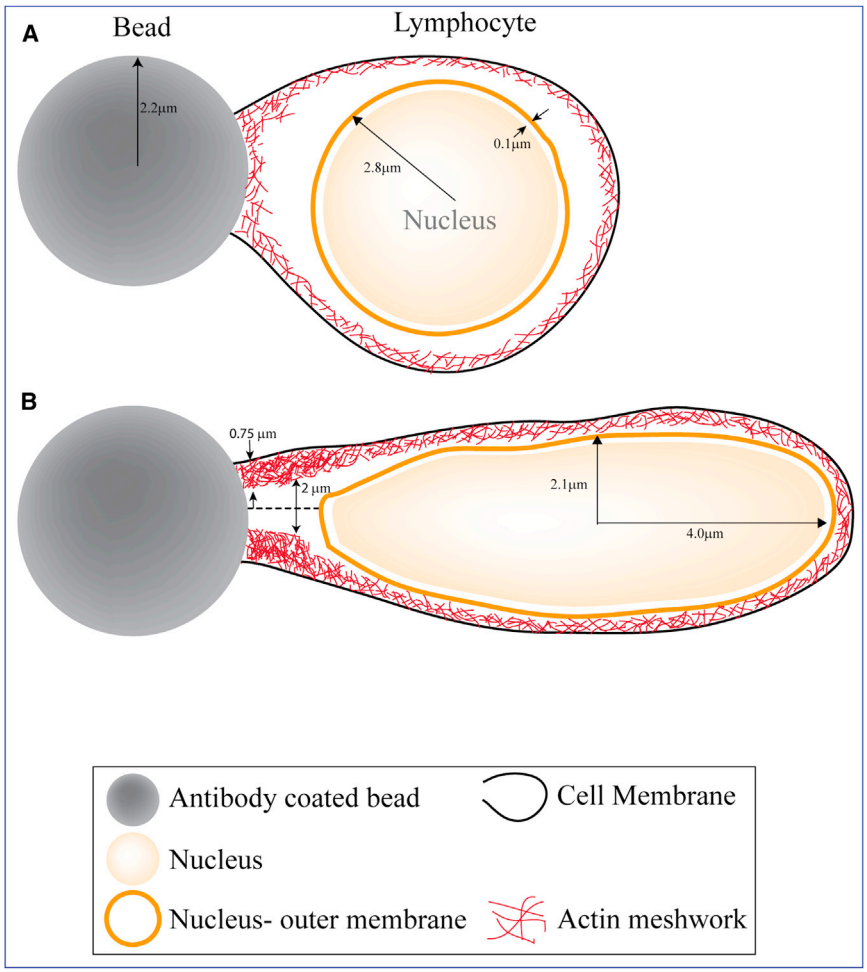

FIGURE 1 Illustration of the process of nuclear deformation in T cells. (*A*) Initial contact between bead and T cell. (*B*) Onset of actin polymerization and nuclear deformation.

receptor activation. The hollow actin cylinder subsequently grows as a result of polymerization at the cell-bead interface and engulfs the nucleus. This leads to an elastic deformation of the latter into an elongated shape.

We substantiate this model by presenting a computational analysis of nuclear deformation induced by a cylindrical actin layer that was characterized by realistic actin density values, and elastic parameters. The model reproduces the observed shapes of deformed nuclei and makes predictions about the mode of actin polymerization, triggered by the activated T-cell receptors, and also about the values of elastic moduli of the nuclear envelope. We present partial experimental support of the model assumptions by visualizing the distribution of polymerized actin within the cell and its nucleus, when in the deformed state.

QUALITATIVE MODEL

Based on the observations above, and the existing phenomenology on T-cell-activation-induced actin polymerization (16,17), we propose a model to explain nuclear deformation after T-cell stimulation by a bead coated with surrogate antigens. Activation of cell receptors results in a massive repolymerization of actin at the bead-cell interface. This is accompanied by remodeling of the submembrane actin network. The repolymerization of actin gives rise to an actin layer that has the shape of a hollow cylinder. The base of the cylinder rests on the circular cell-bead interface and the cross-section dimension is determined by the bead size (Fig. 1). Since the nuclear radius is larger than the internal radius of the growing actin cylinder, the nucleus and the actin layer mutually deform. The nucleus becomes compressed by the actin layer and elongated in the direction of the cylindrical axis. The actin layer, on the other hand, is bulged by the nucleus and its thickness changes as a result of the bulging deformation.

We suggest the following specific scenario for the intermediate stages during the evolution of the system. After receptor activation, the actin cylinder starts growing from the cell-bead contact zone, where new actin monomers are added to the filaments constituting the layer. It subsequently elongates until its free edge reaches the nucleus. During the next stage of cylinder growth, the nucleus is pushed by elongating the actin cylinder's free edge toward the cell pole opposite the bead until it touches the plasma membrane. The subsequent stretching of the plasma membrane prevents

further movement of the nucleus. At the next stage, the continuously growing actin cylinder engulfs the nucleus, leading to deformations of both the nucleus and the actin cylinder. The forces pushing the actin cylinder, and enabling the nucleus and actin layer deformations, are produced by actin polymerization at the cell-bead interface.

Our goal is to compute the mutual elastic deformations of both the cylindrical actin layer and the nucleus. By comparing the calculated nuclear shapes with the observed ones, we will determine the elastic characteristics of the nuclear envelope and estimate the forces generated by actin polymerization at the cell-bead interface.

PHYSICAL MODEL AND COMPUTATIONAL ANALYSIS STRATEGY

We model the preferred shape of the polymerizing actin layer as an elastic cylindrical layer with a thickness of 0.75 μm and an internal radius of 1 μm (Fig. 1). The images supporting this assumption are presented in the Experimental Support section below. The elastic moduli of the actin network constituting the layer are taken to correspond to the average values determined for actin gels: $E = 10$ kPa for Young's modulus (20–22) and $\nu = 0.4$ for the Poisson ratio (23–25).

The nuclear shell is modeled to be spherical in its relaxed state with the internal and external radii equal to 2.7 μm and 2.8 μm, respectively. The elastic moduli, E_s and ν_s, of the lamin network constituting the shell have not been directly measured and therefore will be considered as free parameters whose values will be found from fitting the experimental data.

We do not assume constancy of either the outer area of the elastic shell representing the nucleus or the volume bound by this shell.

The technical complexity of the analysis is twofold. First, the diameter of the spherical shell representing the nucleus is about three times larger than the inner diameter of the actin cylinder. As a result, either the shell or the cylindrical layer, or both of them, must undergo a large deformation leading to strain, with characteristic values that can be estimated as $\varepsilon_{\langle\theta\theta\rangle} = u_r/r \sim 50 - 120\%$, where r and θ denote the radial and angular coordinates in the cylindrical coordinate system related to the symmetry axis of the actin layer, and u_r is the radial component of the displacement vector (26). Hence, the deformation analysis cannot be performed in the linear elastic regime and we use a Neo-Hookean hyperelastic model (27) implemented with the finite-element method (see Supporting Material).

The second complexity is related to the fact that, according to the observations, both the shell representing the nucleus and the cylindrical actin layer are strongly deformed, meaning their effective rigidities are comparable.

The computations have been performed by using Comsol Multiphysics software as described in the Supporting Discussion.

EXPERIMENTAL SUPPORT

To support the model assumptions, we stimulated T cells in vitro by incubating them with surrogate antigens that activate T-cell receptors, namely, αCD3 and αCD28 antibodies (see Supporting Material, for the experimental methods used). For our experiments, we used 4.5-μm-sized superparamagnetic polymer beads that are coated with these surrogate antigens. It has previously been shown that T-cell activation resulting from such stimulation is very similar to that occurring in in vivo conditions (28). Naïve T cells were isolated from H2B-EGFP transgenic mice and activated with antibody-conjugated beads. The resulting whole-cell and nuclear shape transformations were recorded as movies (Movie S1). Time-lapse images of one such representative experiment are shown in Fig. 2. To assess the organization of actin in cells at different stages of the deformation process, rhodamine-phalloidin was used to label the polymerized actin (F-actin). The changes in shape of the polymerized actin layer, corresponding to the stages of both nuclear and cell deformation, are presented in Fig. 3. As shown in Figs. 2 and 3, the cell and the nucleus have nearly spherical shapes before stimulation (Fig. 2) while F-actin forms a thin shell between the cell surface and the nucleus (Fig. 3). After the establishment of a contact between the cell and the bead, both the nucleus and the cell become progressively more elongated (Fig. 2). Also, the polymerized actin layer undergoes a considerable rearrangement (Fig. 3), adopting an elongated shape engulfing the nucleus. In the region between the bead interface and the nuclear contact, the actin layer appears as a hollow cylinder with a cross-sectional radius increasing toward the nucleus (Figs. S1 and S2). The thickness of the actin layer is nonhomogeneous. This was established by drawing a line over the actin images and calculating the full width at half maximum from the corresponding intensity plot to a diffraction-limited resolution (Fig. S2). In the region close to the cell-bead contact, the layer is considerably thicker than in the initial state preceding cell activation and becomes thinner near, and surrounding, the nucleus (Fig. S2). The deformation and rearrangement of the whole system occurs within a few hundred seconds after the formation of a contact.

RESULTS

Equilibrium shapes and elastic moduli

The shapes that were computed for the elastic shell representing the nucleus, and for the engulfing cylindrical elastic layer representing the hollow actin cylinder, are shown for gradually increasing values of the Young's modulus of the shell, E_s (Fig. 4). The color code corresponds to values of the elastic energy density measured in kJ/m^3. Using the entire collection of computed equilibrium shapes for different values of the elastic modulus, E_s and ν_s, we

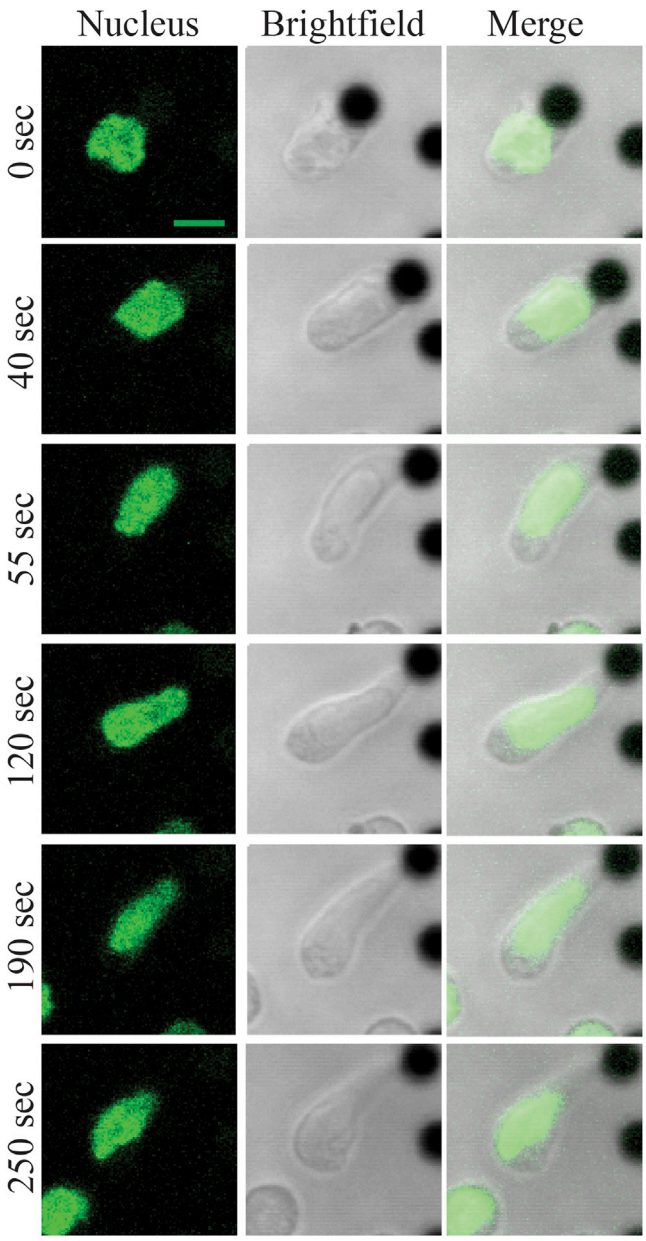

FIGURE 2 Representative time-lapse images of a naïve T cell during activation with an antigen-coated bead. *Green*, H2B EGFP nucleus; antigen-coated beads-*black*. Scale bar, 5 μm. To see this figure in color, go online.

generated two diagrams that describe the expected values of semiaxes of the deformed shell's final shape (Fig. 5). The first diagram (Fig. 5 *A*) displays axes in absolute values, whereas the second diagram (Fig. 5 *B*) shows the same data as a dimensionless ratio of the polar and equatorial radii.

The obtained shapes have to be compared with the typical shape of the experimentally observed deformed nuclei (see Experimental Support) (Fig. 6). The maximum aspect ratio of experimentally observed deformed nuclei is close to 2:1 (Figs. 6 *B* and S3). The best fitting of the computed shapes to observed shapes (Fig. 6 *A*) predicts the shell elastic moduli to be $E_s \sim 60$ kPa and $\nu_s > 0.3$. The value obtained for the Young's modulus, E_s, can be compared with the results from previously reported experiments on giant *Xenopus* oocytes, according to which the value of the two-dimensional Young's modulus of the nuclear envelope is ~25 mN/m (29). For our system, an effective two-dimensional Young's modulus of the nuclear envelope can be obtained by integrating the determined value of E_s over the ~100 nm thickness of the elastic shell, which gives ~6 mN/m. Hence, the nuclear envelope of T cells appears to be somewhat softer than that of *Xenopus* oocytes, which may have numerous causes, including a difference in the thickness and density of the lamin layer.

In addition to overall deformation, our model predicts that the actin layer has to undergo a substantial reduction of thickness in the regions contacting the nucleus. According to our computations, because of the bulging deformation, the thickness of the actin layer changes from 750 nm at the cylinder base, which lies on the cell-bead interface, to values ranging from 500 nm (for a soft nucleus with $E_s = 50$ kPa) to 400 nm (for a stiff nucleus with $E_s = 150$ kPa) in the regions where the actin cylinder contacts the nucleus. These values are in agreement with the data presented in the Experimental Support section above, where the actin layer thickness changes from 750 nm at the actin cylinder base to 410 ± 92 nm at the nucleus contact point (Fig. S4). This agreement provides an additional substantiation of the values obtained for the elastic moduli of the nuclear shell.

The force provided by actin polymerization

In our model, the force, f, pushing the cylindrical actin layer toward the nucleus and driving the engulfment of the nucleus and its deformation is produced by actin polymerizing against the cell-bead interface. This occurs by a mechanism analogous to that of force generation at the leading edge of a moving cell (30,31). A qualitative consideration shows that the force needed to deform the nucleus continuously increases during the early stages of the engulfing process and reaches its maximal value, f_{max}, when the free edge of the actin cylinder attains the equator of the nuclear shape. The further stages of engulfing require lower values of force, and the force vanishes with completion of the nucleus coverage by the actin layer. Hence, the force requirements of nucleus engulfment and deformation are determined by the maximal force, f_{max}.

Calculation of the force values needed for the intermediate stages of the engulfing process turned out to be technically unfeasible (see Supporting Material). However, we were able to compute the equilibrium shapes of the nucleus and the actin layer corresponding to complete engulfment. Our analysis showed that these shapes represent a good approximation for the shapes corresponding to half

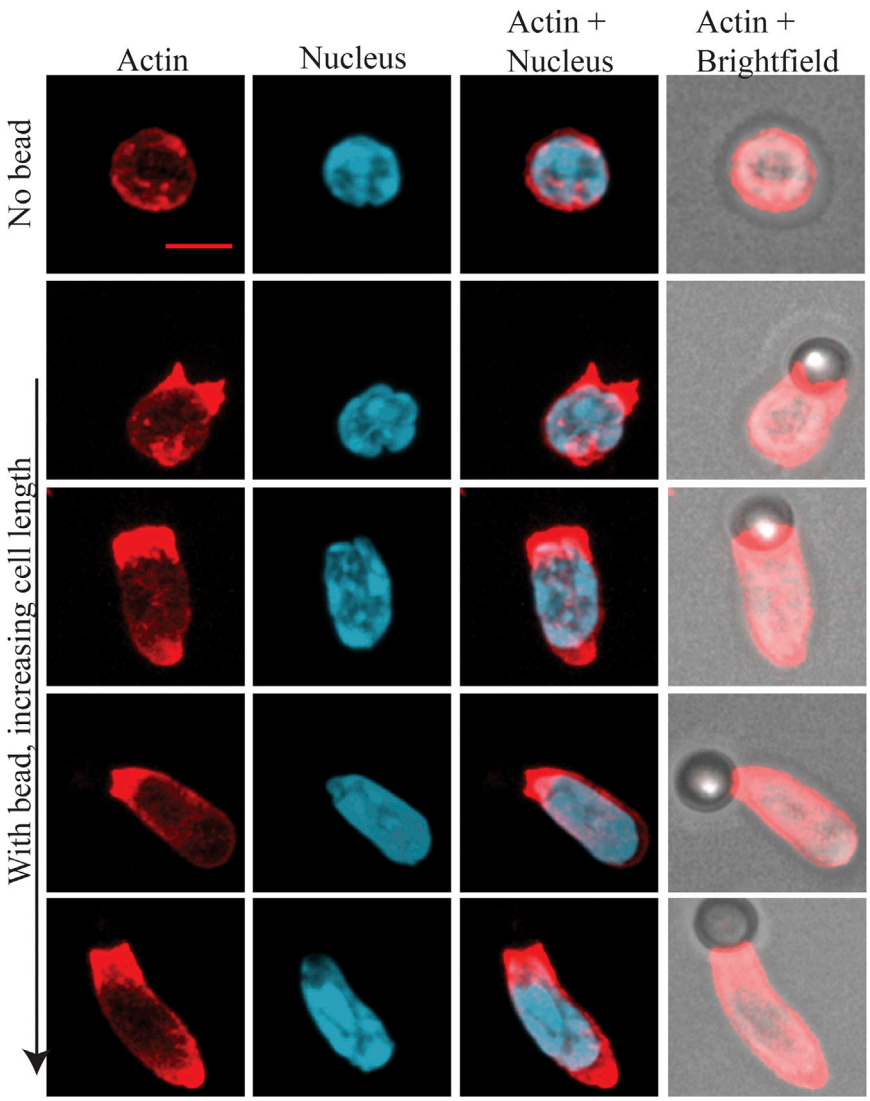

FIGURE 3 Three-dimensional projection image of actin (*red*), nucleus (*blue*), and bright field in a cell without bead (*No bead*) and cells activated with beads and at different extents of nuclear deformation (*With bead, increasing cell length*). Scale bar, 5 μm. All images were acquired 30 min after incubating cells with beads. The orientation of actin structure and nucleus should be noted with respect to bead position seen in the bright-field image. To see this figure in color, go online.

engulfment and therefore can be used for calculation of the maximal force, f_{max} (see Supporting Material). The values of f_{max} computed in this approximation are presented in Fig. S8 *A* in dependence on the Young's modulus of the nuclear shell, E_s. For the relevant values of E_s = 60–100 kPa, the predicted force constitutes ~10 nN.

The obtained values of the force f_{max} enable an estimation of the required density of actin filaments within the cylindrical layer. We assume that each actin filament end polymerizing against the cell-bead interface develops a 1 pN force. This implies that the polymerization force is close to the stalling value of 0.8–1.5 pN (32), because of the substantial resistance to the polymerization process provided by deformation of the actin layer around the nucleus. Based on the measurements, we take the ringlike cross-section area of the cylindrical actin layer at the interface with the bead to be ~6.5 μm^2. According to our computations, creation of the best-fitted nuclear shape requires the generation of 7.6 nN total force, which corresponds to $E_s \sim 60$ kPa and $\nu_s > 0.3$ for the elastic moduli of the nuclear shell. Using the numbers above, we estimate the amount of actin filament ends, ρ_a, that have to polymerize against a unit area of the actin-layer-bead interface to be $\rho_a = 0.0012$ nm^{-2} (see Fig. S8). The value obtained is of the same order of magnitude as the surface density of actin filament ends polymerizing against the leading edge of lamellipodia in moving cells.

DISCUSSION

The major proposal of this study is that changes observed in the shape of the nucleus in T cells activated by adhesion to antibody-coated beads are driven by a repolymerization of the cortical actin layer. This repolymerization results from the activation of T-cell receptors by the surrogate antigens coating the bead.

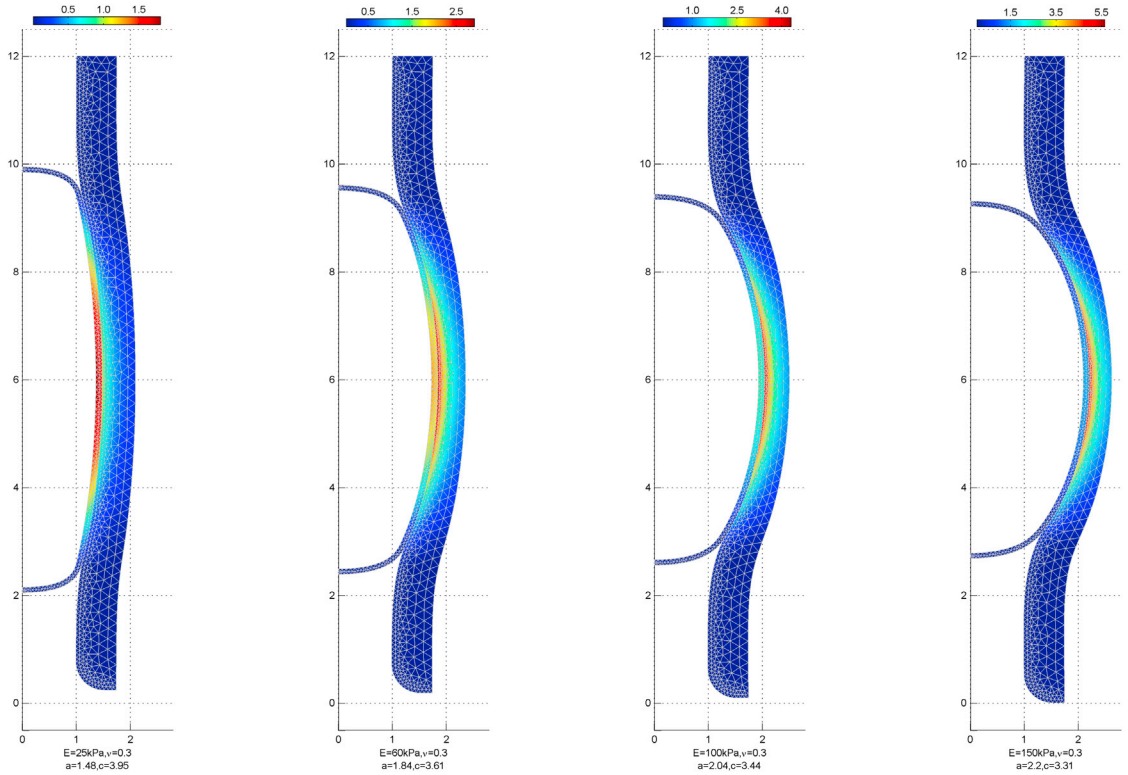

FIGURE 4 Equilibrium shapes (cross-sectional view) of the nucleus and the actin tube for increasing values of the Young's modulus of the nucleus, E_s = 25, 60, 100, and 150 kPa at $\nu_s = 0.3$. The values of the corresponding nucleus semiaxes: equator radius, a, and polar radius, c, are represented in μm below each image. Color bars represent the volume density of the elastic energy measured in kJ/m^3. To see this figure in color, go online.

Specifically, we suggest that activated receptors at the cell-bead interface trigger polymerization of actin filaments, which subsequently form a cylindrical cortical layer that grows within the cell, from the bead towards the nucleus. Since the inner diameter of the actin layer is smaller than that of the nucleus, the layer first pushes the nucleus to the cell plasma membrane, which then retains the nucleus at a fixed position. Further growth of the actin cylinder drives an engulfment of the nucleus, which results in mutual deformation of both the actin cylinder and the nuclear shell and generates strains and elastic stresses within them. Furthermore, the plasma membrane also becomes stretched and stressed.

The proposal of this model was motivated by the results of previous experimental studies that demonstrated, using the drug blebbistatin to inhibit myosin II, or nocodazole to interfere with the polymerization of microtubules, that nuclear deformations are only minimally affected by the

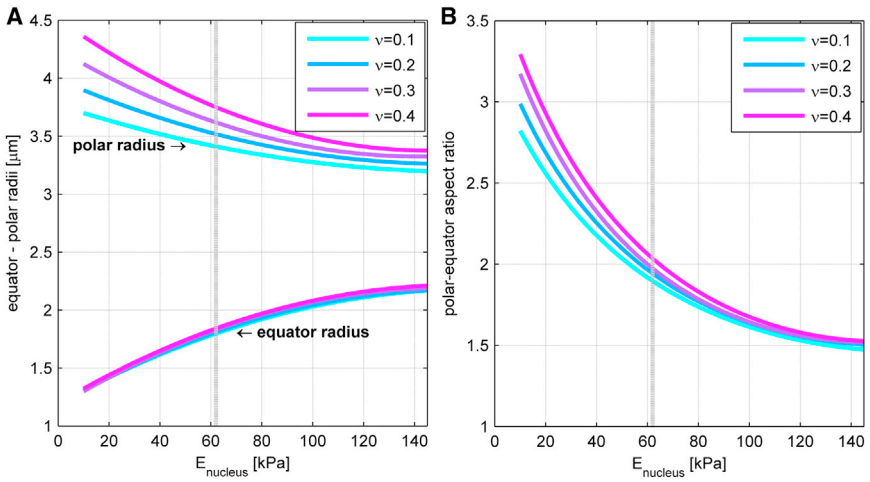

FIGURE 5 Computed dimensions of the nucleus in the semiellipsoidal approximation as a function of the elastic moduli E_s and ν_s. (*A*) Absolute values of the semiaxes of the final deformed nucleus. (*B*) Ratio of the polar radius to the equator radius. The gray dotted line represents the average observed ratio of the axes of the deformed nucleus (2:1) that corresponds to $E_s \sim 60$ kPa and $\nu_s > 0.3$.

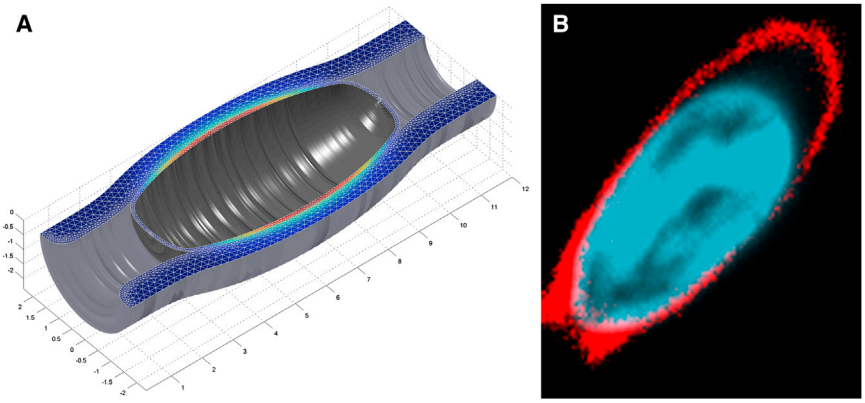

FIGURE 6 Fitting of the computed nuclear shape to the observed shape for the axis ratio 2:1. (*A*) Computed shape for $E_s \sim 60$ kPa and $\nu_s > 0.3$ created by rotation of the second image from the left in Fig. 4. (*B*) Observed shape with fluorescence imaging corresponding to the same axis ratio. *Red*, actin; *blue*, nucleus. To see this figure in color, go online.

inhibition of myosin II motors (19). At the same time, polymerization of actin was essential for nuclear deformation, since treatment with cytochalasin D inhibited this process.

We substantiated this proposal with computations demonstrating that the experimentally observed nuclear shapes, as well as the shape of the surrounding layer of polymerized actin, can be explained based on a purely elastic model. These shapes result from an interplay between the elastic stresses developed within a cylindrical actin layer, which represents the repolymerized cortical actin, and an elastic shell, which represents the nucleus. According to the model, the force responsible for generation of these stresses and deformations is produced by actin polymerization at the cell-bead interface. Computation of this force (~7.6 nN) from fitting the theoretically predicted nuclear shapes to those observed, and a related estimation of the required actin filament density within the cylindrical layer (~0.0012 polymerizing filament ends/nm^2 of the cell-bead interface) indicated that the layer has to be approximately as dense as the familiar actin networks being formed, for example, in the lamellipodia of moving cells.

We provide experimental support for some of the assumptions made in the model by visualizing, in parallel with the changes in nuclear and cell shape, the structural transformations of the actin cytoskeleton. We provide evidence that, indeed, upon receptor activation, actin undergoes massive polymerization next to the cell-bead interface, and the resulting actin layer can be presented as a cylinder that is partially deformed because of nuclear engulfment and has the predicted homogeneity in thickness.

It is tempting to speculate that the stretching of the plasma membrane, which accompanies the whole process, might play a role in a periodic relaxation, and subsequent new deformation, of the nuclear shapes observed in T cells (19). Stresses generated in the plasma membrane may result in the opening of mechanosensitive calcium channels within the membrane, which would in turn trigger depolymerization of the actin cylinder, and restoration of the initial nuclear and cell shapes. The following relaxation in the stress of the membrane would result in closure of the calcium channel and renewed polymerization of the actin cylinder from the cell-bead interface and hence would initiate a new cycle of nuclear deformation.

It has to be noted that, according to our computations, the deformation of the nuclear shell was accompanied by a shrinking of its external area. This implies an emerging area mismatch between the lamin network constituting the shell and the nuclear envelope. We suggest that this mismatch results in the nuclear envelope folding between discrete spots where it is connected to the lamina. According to our estimations, the overall bending energy of the nuclear envelope membrane that results from such folding is about three orders of magnitude lower than the lamina compression energy and therefore can be neglected.

In conclusion, we emphasize that our work should not be seen as a thorough cell biological study providing full experimental proof of the mechanism, but rather as a theoretical biophysical study that suggests, to the best of our knowledge, a novel mechanism and substantiates it computationally.

SUPPORTING MATERIAL

Eight figures, one movie, references (33–35), Supporting Discussion, and Supporting Methods are available at http://www.biophysj.org/biophysj/supplemental/S0006-3495(13)00809-6.

We thank Alex Mogilner and Alexander Bershadsky for discussions of the model and Apurva Sarin for discussions regarding the T-cell experiments.

M.M.K. is supported by the Israel Science Foundation (ISF) (grant No.758/11) and the Marie Curie network Virus Entry, and holds the Joseph Klafter Chair in Biophysics. S.G. and G.V.S. thank the Mechanobiology Institute, National University of Singapore, for financial support. M.M.K. thanks the Mechanobiology Institute, National University of Singapore, for hospitality.

REFERENCES

1. Dahl, K. N., A. J. Ribeiro, and J. Lammerding. 2008. Nuclear shape, mechanics, and mechanotransduction. *Circ. Res.* 102:1307–1318.

2. Rowat, A. C., J. Lammerding, and J. H. Ipsen. 2006. Mechanical properties of the cell nucleus and the effect of emerin deficiency. *Biophys. J.* 91:4649–4664.

3. Brandt, A., F. Papagiannouli, …, J. Grosshans. 2006. Developmental control of nuclear size and shape by Kugelkern and Kurzkern. *Curr. Biol.* 16:543–552.
4. Kumar, A., and G. V. Shivashankar. 2012. Mechanical force alters morphogenetic movements and segmental gene expression patterns during *Drosophila* embryogenesis. *PLoS ONE.* 7:e33089.
5. Bhattacharya, D., S. Talwar, …, G. V. Shivashankar. 2009. Spatio-temporal plasticity in chromatin organization in mouse cell differentiation and during *Drosophila* embryogenesis. *Biophys. J.* 96:3832–3839.
6. Pajerowski, J. D., K. N. Dahl, …, D. E. Discher. 2007. Physical plasticity of the nucleus in stem cell differentiation. *Proc. Natl. Acad. Sci. USA.* 104:15619–15624.
7. Shivashankar, G. V. 2011. Mechanosignaling to the cell nucleus and gene regulation. *Annu. Rev. Biophys.* 40:361–378.
8. Khatau, S. B., S. Kusuma, …, D. Wirtz. 2012. The differential formation of the LINC-mediated perinuclear actin cap in pluripotent and somatic cells. *PLoS ONE.* 7:e36689.
9. Talwar, S., A. Kumar, …, G. V. Shivashankar. 2013. Correlated spatio-temporal fluctuations in chromatin compaction states characterize stem cells. *Biophys. J.* 104:553–564.
10. Khatau, S. B., C. M. Hale, …, D. Wirtz. 2009. A perinuclear actin cap regulates nuclear shape. *Proc. Natl. Acad. Sci. USA.* 106:19017–19022.
11. Mazumder, A., and G. V. Shivashankar. 2010. Emergence of a prestressed eukaryotic nucleus during cellular differentiation and development. *J. R. Soc. Interface.* 7(*Suppl. 3*):S321–S330.
12. Versaevel, M., T. Grevesse, and S. Gabriele. 2012. Spatial coordination between cell and nuclear shape within micropatterned endothelial cells. *Nat. Commun.* 3:671.
13. Roca-Cusachs, P., J. Alcaraz, …, D. Navajas. 2008. Micropatterning of single endothelial cell shape reveals a tight coupling between nuclear volume in G1 and proliferation. *Biophys. J.* 94:4984–4995.
14. Lombardi, M. L., D. E. Jaalouk, …, J. Lammerding. 2011. The interaction between nesprins and sun proteins at the nuclear envelope is critical for force transmission between the nucleus and cytoskeleton. *J. Biol. Chem.* 286:26743–26753.
15. Starr, D. A., and H. N. Fridolfsson. 2010. Interactions between nuclei and the cytoskeleton are mediated by SUN-KASH nuclear-envelope bridges. *Annu. Rev. Cell Dev. Biol.* 26:421–444.
16. Billadeau, D. D., J. C. Nolz, and T. S. Gomez. 2007. Regulation of T-cell activation by the cytoskeleton. *Nat. Rev. Immunol.* 7:131–143.
17. Burkhardt, J. K., E. Carrizosa, and M. H. Shaffer. 2008. The actin cytoskeleton in T cell activation. *Annu. Rev. Immunol.* 26:233–259.
18. Bunnell, S. C., V. Kapoor, …, L. E. Samelson. 2001. Dynamic actin polymerization drives T cell receptor-induced spreading: a role for the signal transduction adaptor LAT. *Immunity.* 14:315–329.
19. Gupta, S., N. Marcel, …, G. V. Shivashankar. 2012. Role of actin dependent nuclear deformation in regulating early gene expression. *PLoS ONE.* 7:e53031.
20. Fujiwara, I., S. Suetsugu, …, S. Ishiwata. 2002. Visualization and force measurement of branching by Arp2/3 complex and N-WASP in actin filament. *Biochem. Biophys. Res. Commun.* 293:1550–1555.
21. Gerbal, F., P. Chaikin, …, J. Prost. 2000. An elastic analysis of *Listeria monocytogenes* propulsion. *Biophys. J.* 79:2259–2275.
22. Laurent, V. M., S. Kasas, …, J. J. Meister. 2005. Gradient of rigidity in the lamellipodia of migrating cells revealed by atomic force microscopy. *Biophys. J.* 89:667–675.
23. Mahaffy, R. E., S. Park, …, C. K. Shih. 2004. Quantitative analysis of the viscoelastic properties of thin regions of fibroblasts using atomic force microscopy. *Biophys. J.* 86:1777–1793.
24. Schmidt, F. G., F. Ziemann, and E. Sackmann. 1996. Shear field mapping in actin networks by using magnetic tweezers. *Eur. Biophys. J.* 24:348–353.
25. Wagner, O., H. Schüler, …, J. Bereiter-Hahn. 2001. Sound attenuation of polymerizing actin reflects supramolecular structures: viscoelastic properties of actin gels modified by cytochalasin D, profilin and α-actinin. *Biochem. J.* 355:771–778.
26. Landau, L. D., E. Lifshitz, …, A. M. Kosevich. 1986. Theory of Elasticity. Elsevier, Philadelphia.
27. Simo, J. C., and K. S. Pister. 1984. Remarks on rate constitutive equations for finite deformation problems: computational implications. *Comput. Methods Appl. Mech. Eng.* 46:201–215.
28. Trickett, A., and Y. L. Kwan. 2003. T cell stimulation and expansion using anti-CD3/CD28 beads. *J. Immunol. Methods.* 275:251–255.
29. Dahl, K. N., S. M. Kahn, …, D. E. Discher. 2004. The nuclear envelope lamina network has elasticity and a compressibility limit suggestive of a molecular shock absorber. *J. Cell Sci.* 117:4779–4786.
30. Mogilner, A., and G. Oster. 1996. Cell motility driven by actin polymerization. *Biophys. J.* 71:3030–3045.
31. Mogilner, A., and G. Oster. 2003. Force generation by actin polymerization II: the elastic ratchet and tethered filaments. *Biophys. J.* 84:1591–1605.
32. Footer, M. J., J. W. Kerssemakers, …, M. Dogterom. 2007. Direct measurement of force generation by actin filament polymerization using an optical trap. *Proc. Natl. Acad. Sci. USA.* 104:2181–2186.
33. Attard, M. M. 2003. Finite strain—isotropic hyperelasticity. *Int. J. Solids Struct.* 40:4353–4378.
34. Holzapfel, G. 2000. Nonlinear Solid Mechanics: A Continuum Approach for Engineering. John Wiley and Sons, New York.
35. Truesdell, C., and W. Noll. 2004. The Non-Linear Field Theories of Mechanics. Springer-Verlag, Berlin/Heidelberg/New York.

Model of T-cell nuclear deformation by the cortical actin layer

Running Title: Actin mediated nuclear deformation

Gur Fabrikant[1,3], Soumya Gupta[2,3], GV Shivashankar[2]*, and Michael M Kozlov[1]*

[1]Department of Physiology and Pharmacology, Sackler Faculty of Medicine, Tel Aviv University, Ramat Aviv, 69978 Tel Aviv, Israel

[2]Mechanobiology Institute & Department of Biological Sciences, National University of Singapore, Singapore

[3]these authors contributed equally to this work

* Correspondence: shiva.gvs@gmail.com, michk@post.tau.ac.il

Supplementary information

Method of computations

Equilibrium shapes and elastic moduli

To describe the mutual deformation of the actin layer and the elastic shell representing the nucleus, we use the modified (compressible) Neo-Hookean model for isotropic materials (see derivation in [1],[2]).

The strain energy functional is given by:

$$\psi = \frac{1}{2}\mu\left(I_1 - 3\right) - \mu \ln J + \frac{1}{2}\lambda\left(\ln J\right)^2 \qquad \textbf{(1)}$$

where μ, λ are the Lame' coefficients which can be expressed through Young and Poisson moduli according to: $\mu = E/2\left(1+\nu\right)$ and $\lambda = E\nu/(2\left(1-2\nu\right)\left(1+\nu\right))$.

The isochoric and dilatational deformations are functions of the principal invariants of the right Cauchy strain tensor, C [3,4], which are $I_1 = Tr\left(C\right)$ and $J = \det(F_{vol})$.

The equilibrium system configurations correspond to the minimum of the total elastic energy obtained by integration of (1) over the volume. The energy minimization was performed based on the weak form or virtual displacement principle according to standard Finite Element methods. To match the computed shapes of the nucleus shell and the actin layer (see below), we used the Lagrange-quadratic shape functions on

top of a triangular mesh which was manually refined towards the contact region between the two sub-systems. The assembly and solution were carried out by an Augmented Newton solver - available within the commercial software Comsol Multiphysics.

The first step and the main idea, was to make an educated guess of the possible shapes of the contact region between the two elastic bodies based on their initial unstressed shapes and (axial) symmetry. The simplest deformation contours for spherical compressions are elliptical arcs, thus a family of ellipsoids was used to approximate the equilibrium contour at the contact region. Second, we segregated the system into two complementary sub-systems (see Fig. S5): one representing the nucleus shell and the second modeling the cylindrical actin layer. The nucleus shell was compressed by an infinitely rigid concave scaffold to a final prolate ellipsoid with a pre-defined final equator radius. The actin layer was expanded by an infinitely rigid ellipsoid whose equator radius, *a*, equals that of the scaffold (see Fig. S5). In order to determine the tuning range for the ellipsoid polar radius, we noted that any isotropic shell under radial compression experiences a reduction of its area. For each value of the equator radius, *a*, we used an initial polar radius, *c*, that preserves the original nucleus area, A_{tot}, according to:

$$A_{tot} = 2\pi a^2 \left(1 + \frac{\cos^{-1}(a/c)}{(a/c)\sqrt{1-(a/c)^2}} \right) \quad \textbf{(2)}$$

We then changed the shape of the ellipsoid by reducing *c* until the shapes of the deformed nucleus shell and actin layer coincided in all contact points. The resulting configuration represented a "contact ellipsoid" which was still not the correct solution for the whole system. Among all "contact ellipsoids", only the configuration that corresponded to a global minimum of the strain energy could be regarded as a physical solution. Thus in order to find the correct solutions, we recorded the "contact ellipsoid" dimensions, integrated over the elastic strain energies separately in both sub-systems and summed up the results into a total strain energy value $E_{tot} = \iiint_{nucleus} W_s dv + \iiint_{tube} W_s dv$.

By repeating this procedure with different elastic moduli for different values of the equator radii, we created the energy curves seen in Fig. S6. Note that the energy was calculated with respect to a global non-stressed state represented by the nucleus radius

equal to $2.8\mu m$ and the inner radius of the actin cylinder equal to $1\mu m$. The minimum of each curve in Fig. S6 represents a global minimum of the system energy, hence defining the equilibrium shape of the nucleus and tube for a given choice of elastic moduli- E,ν.

Estimation of the maximal forces and filament density at the cylindrical base of the polymerizing actin gel

The maximum axial reaction force, needed for engulfing the nucleus, occurs when the nucleus is covered to its midst by the actin tube. Due to convergence problems of the used computer program, we were unable to compute directly the exact equilibrium shapes for partial engulfing. Therefore, we used the equilibrium shapes received for complete engulfing as an approximation for the shapes corresponding to half engulfing and used them for calculating the reaction forces that act from the bead to the base of the actin tube, which represent the force developed by actin polymerization.

Essentially, all elasticity-based contact problems admit two possible ways of calculating the overall reaction forces on some fixed boundary, direct and indirect ones. In the direct approach, the reaction (or polymerization) force on the bead can be calculated directly by integrating the axial stress component of the actin tube at the "fixed" cylindrical base ($z=12$): $f_z = \iint\limits_{A-bead} \sigma_{zz} dA$ (blue line Fig S7B). This force varies greatly as the nucleus penetrates and deforms the tube. It reaches a maximal value when the nucleus only "pushes in" on the tube– i.e. engulfed till its midst (Fig S7B, blue curve at $\sim Z_{nuc} = 1\mu m$) and reaches ~ zero when the nucleus is fully covered by the tube. In this state, the nucleus "pushes in and out", symmetrically on the tube and the contributions to the overall force in the $\hat{z}$ direction cancel out each other (Fig S7B, blue curve at the lower right corner: $Z_{nuc} = 6\mu m$). Each of the blue triangles, mark a convergent solution which is later used for interpolating the maximal direct force at mid-penetration.

As the elastic moduli of the nucleus increase, thus leading to wider equatorial ellipsoids, the amount of converging points decreases till we are no longer able to properly interpolate the correct location and magnitude of the mid-penetration force.

For these cases, namely stiff nuclei with equilibrium equator radii $a_{eq} > 2\mu m$, we revert to the indirect estimation.

The indirect method suggested for this contact problem, involves the contact pressure profile of the deforming boundary and utilizes the symmetry of the final engulfed state (Fig S7B - red curve). We suggest that the contact pressure over half a nucleus in the final state is roughly the same as the contact pressure felt by the tube in mid-penetration. We therefore calculate the axial reaction force by integrating the $\hat{z}$-projection of the contact pressure profile over half a nucleus in the fully engulfed state: $f_z \approx \iint_{half\ nuc} T^{(n)} \cdot n_z da$. We were able to make sure that the indirect method gives an excellent approximation for the case of nuclei much softer than the actin layer as seen in Fig S7B (the value of the red curve at $z = 6$ approximately coincides with the maximal direct force - blue curve at $z = 1$ in Fig S7B.)

A careful inspection of these contact profiles as seen in Fig S7A, indeed confirms that half of the symmetrical profile at full engulfment ($z_{nuc} = 6\mu m$) is similar in shape and magnitude to the entire profile at mid-penetration ($z_{nuc} \sim 1\mu m$). Moreover, we should emphasize that the only "true" profile among these profiles (Fig S7A) is the fully engulfed configuration ($z_{nuc} = 6\mu m$). "True" in the sense that it corresponds to a state of a total minimal energy and is identical in both parts of the segregated system as required by force balance principle. The other profiles stand for approximated equilibrium shapes. They were measured only on the tube side and are, in general, different for the two sides of the segregated parts of the system.

Taking the mid-penetration force estimates (from Fig S7B) for the entire configurations space for both direct and indirect methods, we construct two concluding diagrams seen in Fig S8. The first diagram represents the total maximal mid-penetration force calculated at the bead surface as a function of the Young's modulus of the nuclear shell E_s. The second diagram represents the result of determination, based on the maximal mid-penetration force, of the number of actin filament end pushing a unit area of the bead. The area per actin filament end is $a_{filament} = A_{tot} / n_{filament}$ where $A_{tot} = \pi\left(1.75^2 - 1\right)\mu m^2$. The number of actin filament ends, $n_{filament}$, is derived by dividing the total force with the assumed force

that each actin filament generates as a result of polymerization ($f_{filament} \sim 1pN$), $n_{filament} = f_z^{tot} / f_{filament}$.

Experimental Methods

Mice cells and their activation

All experiments used C57/Bl6 mice or transgenic B6.Cg-Tg (Hist1H2BB/EGFP) mice. The H2B-EGFP transgenic mouse was purchased from The Jackson laboratory (http://jaxmice.jax.org). These mice express the H2B protein fused to EGFP under the chicken beta-actin promoter coupled to CMV immediate early promoter/enhancer. As a result all nucleated cells in the mouse have fluorescence. $CD4^+$ naïve T-cells were isolated from spleen of 8-10 week old mice using MagCellect isolation kit (R&D Systems, MN). $1X10^5$ cells were stimulated with antigen coated beads (Invitrogen, CA) at a stoichiometry of 1:2 (cell:bead).

Immunostaining

For staining, cells were activated on poly-d-lysine coated glass bottom dishes, fixed with 1% PFA for 20 minutes, permeabilized with 0.2% NP-40 for 5 minutes and blocked with 10mg/ml BSA for 1 hour at room temperature. Actin was stained using rhodamine phalloidin and DNA with Hoechst 33342 (Sigma).

Confocal imaging

Zeiss (LSM510-Meta) or Olympus FV1000 confocal fluorescence microscopes were used for imaging experiments using 63X/ 1.4 N.A oil immersion objective. 8-bit images of 512-by-512 pixels were acquired with 1 airy-unit pinhole aperture size and a z-step size of 500 nm. Time-lapse live cell images were recorded at 5 seconds/frame, with stage temperature maintained at 37^OC and CO_2 concentration maintained at 5%. 488nm laser line was used to excite EGFP or Alexa 488 tagged proteins, 543nm for rhodamine phalloidin and 405nm for Hoechst 33342.

Supporting References

1. Attard MM. 2003. Finite strain—isotropic hyperelasticity. International Journal of Solids and Structures 40(17):4353-4378.
2. Simo JC, Pister KS. 1984. Remarks on rate constitutive equations for finite deformation problems: computational implications. Computer Methods in Applied Mechanics and Engineering 46(2):201-215.
3. Holzapfel G. 2000. Nonlinear Solid Mechanics: A Continuum Approach for Engineering: John Wiley and Sons.
4. Truesdell C, and Noll, W. 2004. The Non-Linear Field Theories of Mechanics: Springer-Verlag Berlin Heidelberg New York

Supplementary Movie S1. Time-lapse imaging of H2B EGFP labeled T-cell activation by surrogate antigen-coated beads. Images were recorded at 5 seconds per frame.

Fig. S1

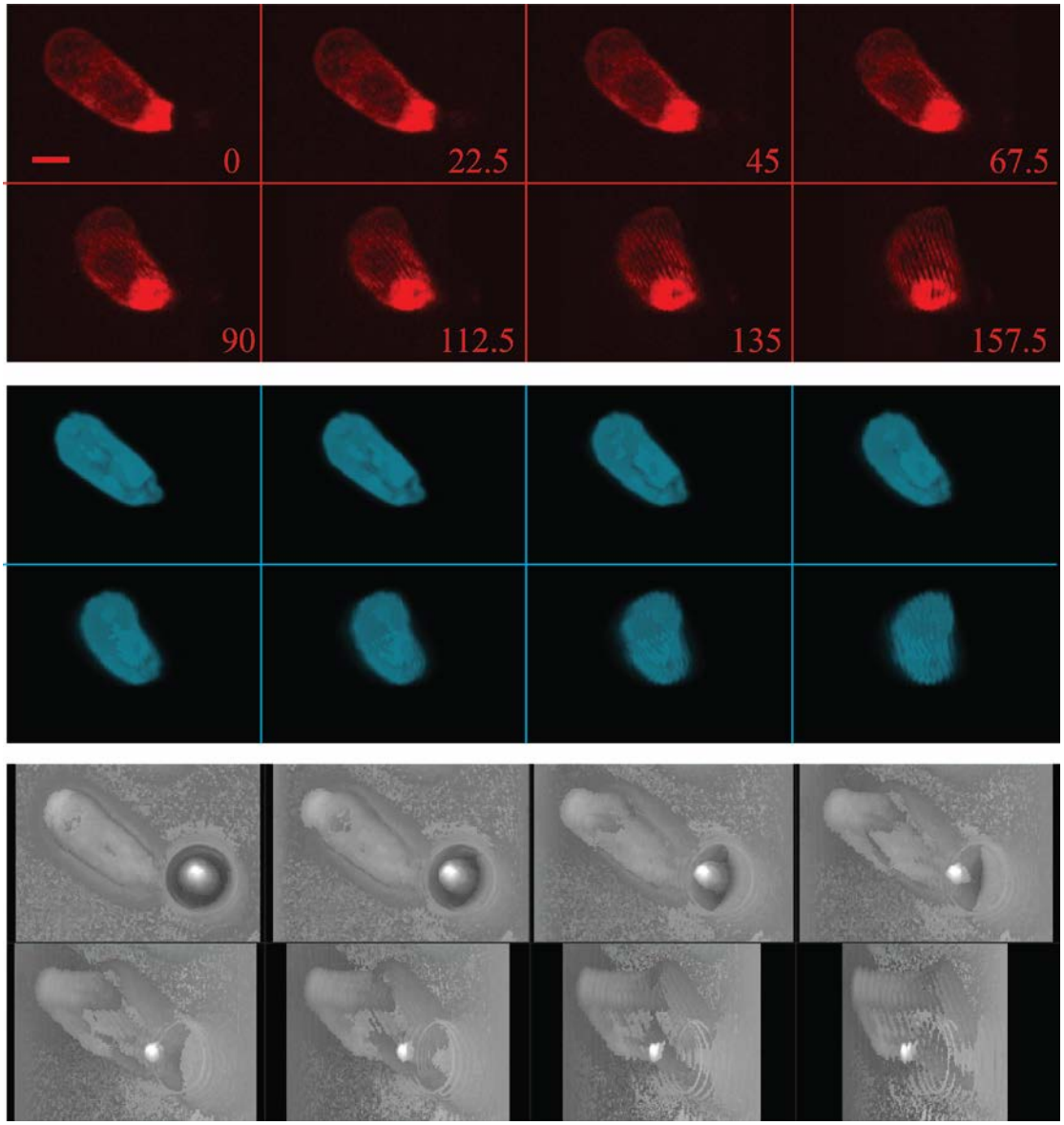

Fig. S1. 3D projection image of actin (red), DNA (blue) and bright-field (grey) for a representative cell with elongated cellular and nuclear architecture depicting the hollow actin tube. The numbers in red indicate the projection angle. Note the position of actin tube with respect to bead position seen in bright-field image. Scale bar 2μm.

Fig. S2

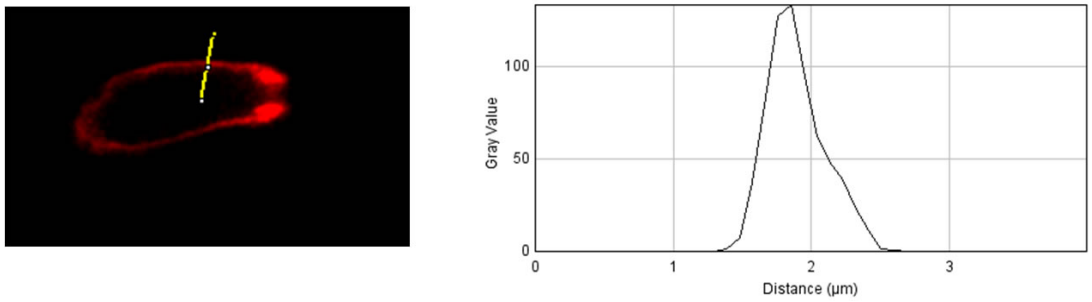

Fig S2. Actin stained image (red) of a T-cell with a line drawn across (yellow) (left panel). The corresponding intensity plot for this line is shown (right panel), from which the thickness of actin layer was determined.

Fig. S3

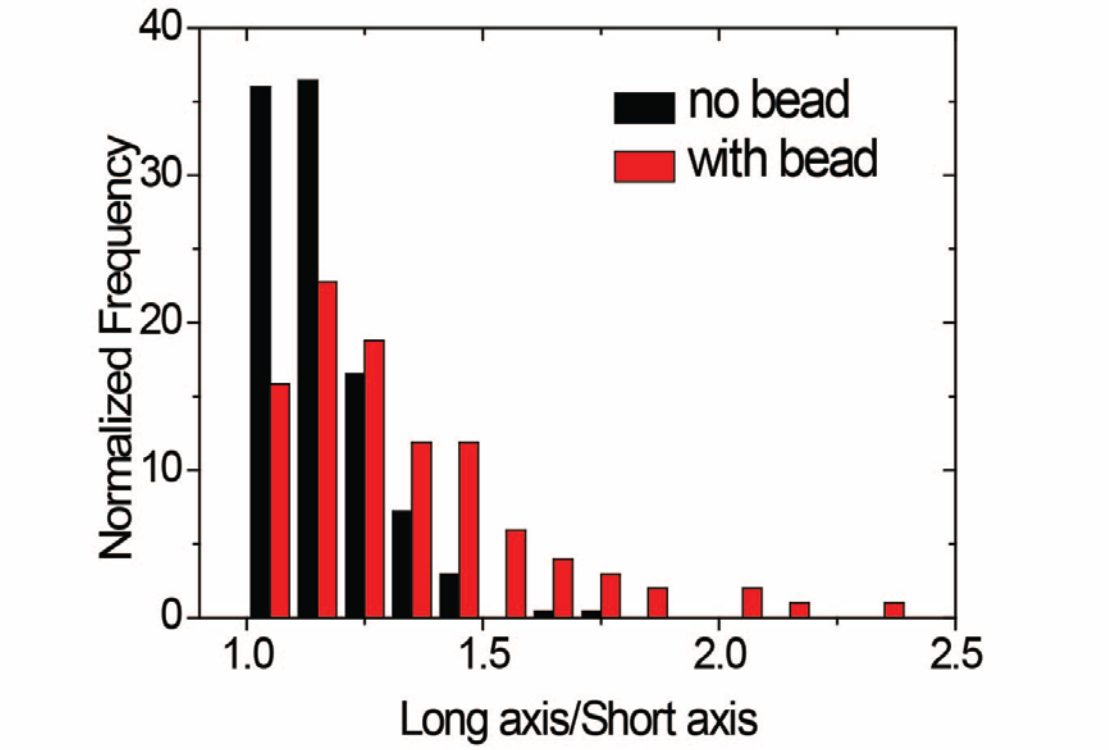

Fig S3. Graph showing the aspect ratio of nucleus for T-cells which do not make contact with bead (black) and those which make contact with beads (red). The maximum nuclear aspect ratio observed was ~2:1.

Fig. S4

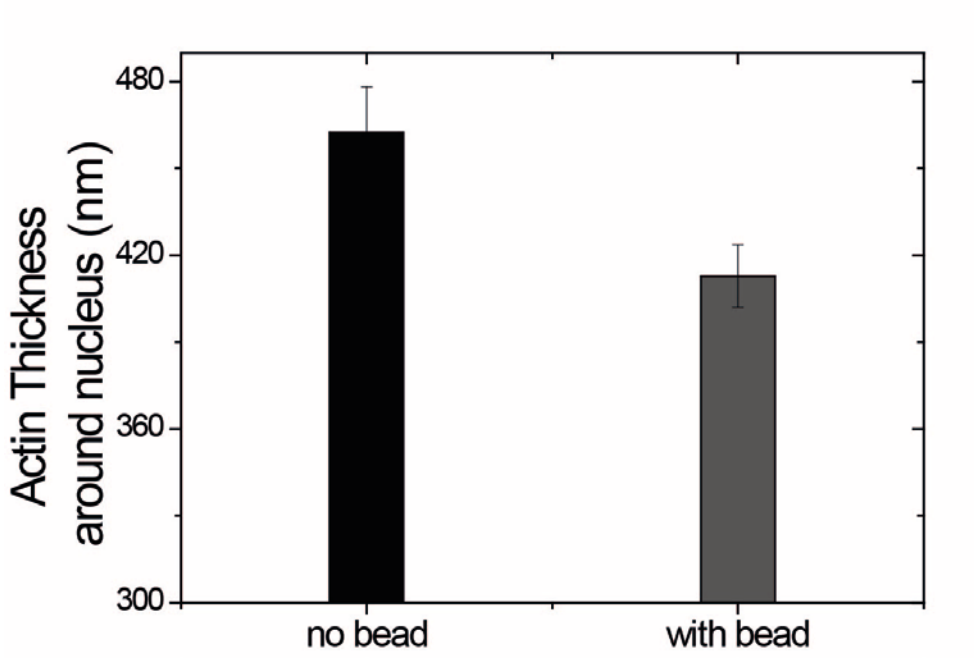

Fig. S4. Thickness of actin layer around the nucleus in cells without bead contact and those with bead contact and deformed nucleus. (n=50-60). SE plotted.

Fig. S5

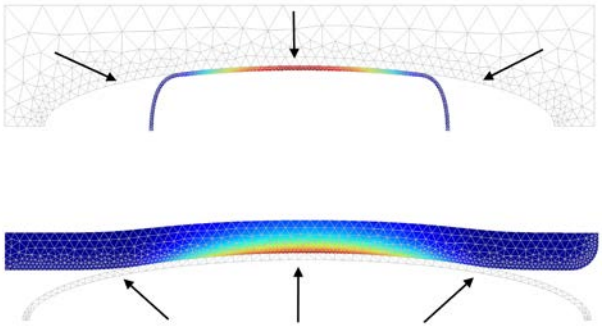

Fig. S5. Splitting the analysis into two complementary parts implemented in Finite Element Method. Lower panel - an infinitely rigid ellipsoid pushing from the inside on the actin tube. Upper panel - an infinitely rigid concave scaffold pressing on the nucleus shell. Both contours are mutually varied till a contact is found.

Fig. S6

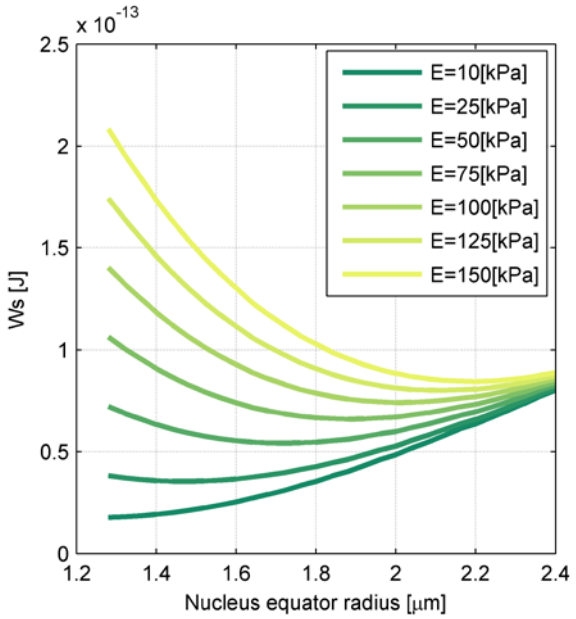

Fig. S6. The dependence of the total elastic strain energy on the final values of the equator radius of the nucleus. Different curves denote different values of the nucleus shell Young's modulus, E_s, for a given Poisson ratio $\nu_s = 0.1$.

Fig. S7

A

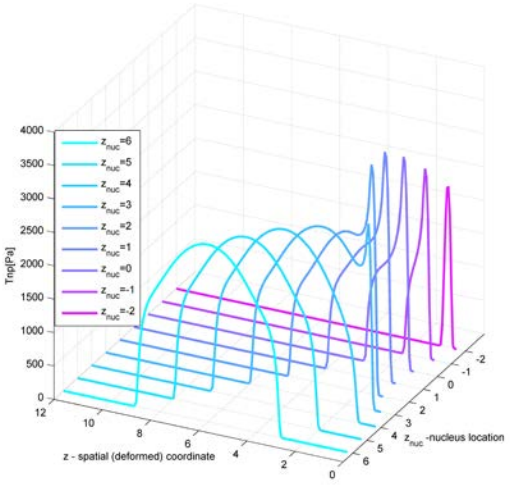

B

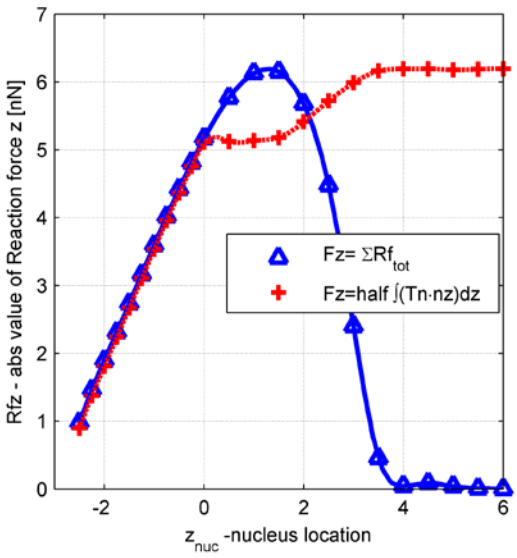

Fig. S7. Estimation of the axial reaction force at the bead surface using direct and indirect methods. (A). Contact pressure profiles measured on the deforming boundary as the nucleus moves away from the center of the actin tube towards the free edge. (B). Mid-penetration reaction force measured in two ways: (i) Directly at the bead surface (blue line) (ii) Indirectly by integration over half the contact pressure profile-projected on the $\hat{z}$ axis (red line). Both parts of the figure were calculated for an equator radius $a = 1.72\mu m$ with elastic moduli $E_s = 50kPa$ and $\nu_s = 0.1$.

Fig.S8

A

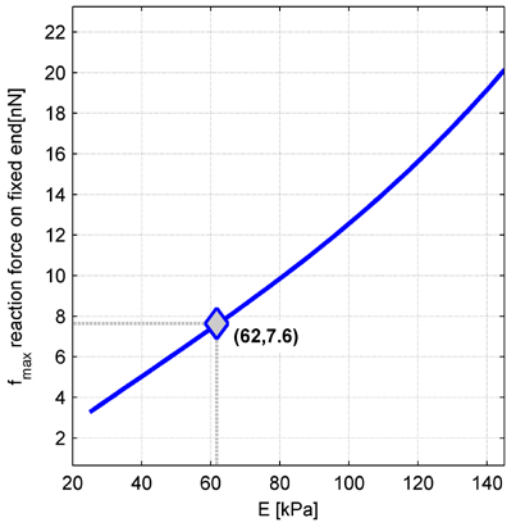

B

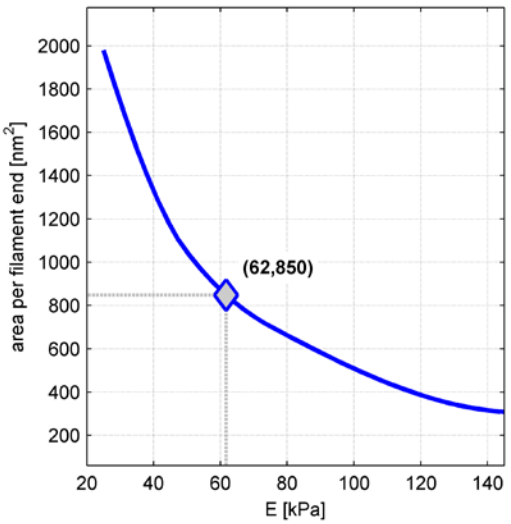

Fig. S8. Maximal force and actin filament spacing at the bead surface as function of the nucleus shell Young's modulus, E_s. The best fitted observed ratio of the deformed nucleus axes (2:1) corresponding to $E_s \sim 60kPa$ is marked on both diagrams. (A). Mid-penetration maximal (axial) reaction force measured in nN. (B). Lateral area per actin filament end at the bead surface in nm^2.